







Noninvasive in vivo photoacoustic detection of malaria with Cytophone in Cameroon

Received: 16 April 2024

Accepted: 7 October 2024

Published online: 25 October 2024


 Check for updates

Aayire C. Yadem^{1,9}, Jillian N. Armstrong^{2,9}, Mustafa Sarimollaoglu^{1,3}, Civian Kiki Massa⁴, Jean-Michel Ndifo⁵, Yulian A. Menyaeov ^{1,3}, Anastasie Mbe^{4,5}, Kacey Richards², Martina Wade², Yushun Zeng ^{6,7}, Ruimin Chen^{6,7}, Qifa Zhou ^{6,7}, Elvis Meten^{4,5}, Rodrigue Ntone⁴, Yves Le Grand Napa Tchuedji⁵, Safi Ullah¹, Ekaterina I. Galanzha^{1,3}, Lucrèce Eteki⁴, Hortense Kamga Gonsu⁵, Alexandru Biris⁸, James Y. Suen^{1,8}, Yap Boum Il^{4,5}, Vladimir P. Zharov^{1,3}  & Sunil Parikh  

Current malaria diagnostics are invasive, lack sensitivity, and rapid tests are plagued by deletions in target antigens. Here we introduce the Cytophone, an innovative photoacoustic flow cytometer platform with high-pulse-rate lasers and a focused ultrasound transducer array to noninvasively detect and identify malaria-infected red blood cells (iRBCs) using specific wave shapes, widths, and time delays generated from the absorbance of laser energy by hemozoin, a universal biomarker of malaria infection. In a population of Cameroonian adults with uncomplicated malaria, we assess our device for safety in a cross-sectional cohort ($n = 10$) and conduct a performance assessment in a longitudinal cohort ($n = 20$) followed for 30 ± 7 days after clearance of parasitemia. Longitudinal cytophone measurements are compared to point-of-care and molecular assays ($n = 94$). Cytophone is safe with 90% sensitivity, 69% specificity, and a receiver-operator-curve-area-under-the-curve (ROC-AUC) of 0.84, as compared to microscopy. ROC-AUCs of Cytophone, microscopy, and RDT compared to quantitative PCR are not statistically different from one another. The ability to noninvasively detect iRBCs in the bloodstream is a major advancement which offers the potential to rapidly identify both the large asymptomatic reservoir of infection, as well as diagnose symptomatic cases without the need for a blood sample.

Significant strides in malaria control have occurred since the millennium due to the availability of insecticide-treated bed nets, effective artemisinin-based combination therapies, and the use of antigen-based rapid diagnostic tests (RDTs)¹. However, gains have stagnated

since 2015, with annual malaria deaths increasing yearly since 2019¹. Almost half of the world's population remains at risk for malaria transmission, with children and pregnant women at the highest risk of morbidity and mortality^{1,2}. *Plasmodium falciparum* (*Pf*) is the species

¹CytoAstra, LLC, Bioventures/UAMS, Little Rock, AR, USA. ²Yale School of Public Health, New Haven, CT, USA. ³Department of Otolaryngology - Head and Neck Surgery, Arkansas Nanomedicine Center, University of Arkansas for Medical Sciences (UAMS), Little Rock, AR, USA. ⁴Epicentre, Yaoundé, Cameroon. ⁵University of Yaoundé I, Yaoundé, Cameroon. ⁶Alfred E. Mann Department of Biomedical Engineering, University of Southern California, Los Angeles, CA, USA. ⁷Department of Ophthalmology, University of Southern California, Los Angeles, CA, USA. ⁸Department of Applied Science & Center for Integrative Nanotechnology Sciences, University of Arkansas at Little Rock (UALR), Little Rock, AR, USA. ⁹These authors contributed equally: Aayire C. Yadem, Jillian N. Armstrong.  e-mail: zharovvladimirp@uams.edu; sunil.parikh@yale.edu

responsible for the majority of disease burden, with *P. vivax* (*Pv*) as the co-dominant species outside of Africa, and *P. malariae* (*Pm*), *P. ovale* species (*Po*), and *P. knowlesi* increasingly reported^{1,3}. RDTs have now surpassed the gold standard, light microscopy, in point-of-care (POC) settings. However, both RDTs and microscopy require blood sampling and have poor sensitivity with limits of detection (LoD) ≥ 50 –100 parasite/ μL (0.001–0.002% parasitemia), which equates to $>10^8$ circulating parasites before parasitemia is detectable^{4,5}. In addition, RDTs are unable to distinguish between all species and are increasingly compromised by the presence of target antigen deletions^{5–9}. Thus, there remains an urgent need for sensitive POC methods that can rapidly detect low level asymptomatic infections, which comprise the bulk of the malaria burden worldwide, as well as speciate and quantify parasitemia¹⁰. Such advancements are essential to achieve malaria elimination and improve control in diverse transmission settings.

Standard nested PCR and loop-mediated isothermal amplification (LAMP) show improved sensitivity (LoD ~ 1 parasite/ μL), and while LAMP is POC, parasite quantification and multiplexing are not yet available, and the approach has had very limited uptake^{11,12}. Highly sensitive quantitative PCR (qPCR) assays targeting genomic DNA (such as 18S ribosomal DNA or var gene acidic terminal sequence (varATS)) or reverse transcriptase qPCR (RT-qPCR) targeting RNA are capable of quantification, can be multiplexed, and are more sensitive (LoD ≤ 16 –60 parasites/mL)^{13–15}. However, PCR-based methods require blood sampling, advanced laboratory infrastructure, qualified personnel, consumables, and have much slower turnaround times, greatly limiting their use in low and middle-income countries for real-time parasite detection.

Hemozoin (Hz), a heme crystal formed following parasite degradation of hemoglobin (Hb) in infected red blood cells (iRBCs), is a common byproduct of development for all *Plasmodium* species^{16–18}. This inert, insoluble biocrystal, also known as malarial pigment, is chemically identical to β -hematin and has unique magnetic and optical properties, making it a potential diagnostic target^{16,17}. There are several approaches under development that use microscopy, optical absorbance, magnetic resonance, and surface-enhanced Raman scattering to detect the distinct physicochemical characteristics of Hz^{19–27}. However, many of these methods have only been assessed using synthetic Hz, either in vitro or ex vivo, and nearly all require a blood sample^{19–27}. A recent Hz-based device has shown comparable ex vivo diagnostic accuracy to light microscopy for both *Pf* and *P. vivax* field-based detection of malaria in blood samples^{28–30}. Because sample extraction for ex vivo analysis is invasive, may alter cell characteristics, and restricts sample volume, which limits the ability to detect low-density infections, in vivo laser-based technology, including near-infrared spectroscopy (NIRS) and photoacoustic (PA) flow cytometry (PAFC) have been proposed as highly-sensitive, noninvasive methods for detecting Hz^{31–36}. A recent proof-of-concept study demonstrated the potential of NIRS combined with machine learning to detect malaria-infected individuals noninvasively³⁶. PAFC is based on the transcutaneous delivery of low-energy laser pulses through intact skin into a blood vessel, where localized heating of Hz nanocrystals occurs due to the higher light absorption of Hz in iRBCs compared to hemoglobin (Hb) in normal RBCs (nRBCs)³⁷. Light absorption leads to the thermoacoustic generation of acoustic waves that are recorded by small ultrasound transducers in acoustic contact with the skin. PAFC can: (1) interrogate a large volume of blood within a short period of time (estimated 0.2–2.0 mL of blood in 10 s)^{38,39}, leading to higher sensitivity over microscopy and RDTs; (2) detect intrinsic absorption noninvasively (no blood draw needed); (3) work label-free (no reagent injection into the blood); and (4) utilize a level of laser energy fluence well-tolerated for biological tissue and blood^{37–39}. For circulating tumor cell (CTC) detection in melanoma patients, we demonstrated a 1000-fold sensitivity improvement over conventional diagnostics^{38,40}. We previously demonstrated the successful application of PAFC for iRBC detection in vitro and in murine malaria models^{37,41}. Here, we present

the results of a cross-sectional and longitudinal diagnostic performance and safety study of Cytophone in adults presenting with and treated for uncomplicated malaria in Yaoundé, Cameroon. This application of a portable prototype PAFC device, called Cytophone, uses a high-pulse-rate laser and ultrasound transducer array for the successful, rapid, noninvasive, in vivo detection of iRBCs in malaria-infected individuals.

Results

Patient profile

Study participant enrollment and follow-up took place from February 21 to November 30, 2020. The study was conducted in two phases, an initial cross-sectional cohort seen at a single visit for Cytophone device optimization and safety (training set), followed by a longitudinal diagnostic performance and safety study cohort (validation set). Study staff recruited adults age ≥ 21 years with uncomplicated malaria confirmed by either RDT or blood smear microscopy from the University Teaching Hospital of Yaoundé or nearby clinics. Sixteen individuals were screened, and 11 participants were enrolled in the cross-sectional cohort. Sixty-nine individuals were screened, and 27 were enrolled in the longitudinal cohort (Supplementary Fig. 1). Of the 47 screen failures, 43 did not meet eligibility criteria, and 4 declined participation. The median age of the 38 enrolled adults was 37 years (range: 21–84); 61% were female, and all except one (97%) were Cameroonian. Additional demographic data for the 10 individuals in the safety assessment and the 20 individuals in the longitudinal assessment are in Supplementary Table 1. Visit windows allowed longitudinal cohort participants to be seen out to day 37 following artemisinin-based combination therapy.

Principle and schematics of the Cytophone

The portable Cytophone prototype uses a 1064-nm compact solid-state laser with a pulse width of 1.5 ns, pulse rate of 1 kilohertz, and adjustable energy level of up to 240 μJ (Fig. 1a–c). The optical system (Fig. 1c) includes a green pilot laser at 532 nm, which was adjusted collinearly to the 1064-nm laser with dichroic mirrors, and an optical tip consisting of spherical and cylindrical lenses for the creation of a linear laser beam (Fig. 1c) as in conventional in vitro flow cytometry³¹.

The thermal expansion of laser-heated Hz in iRBCs generates acoustic waves referred to as PA signals that are detected with ultrasound transducers placed on the skin (Figs. 1a, 2a, Supplementary Fig. 2). For acoustic coupling, water from a small reservoir flows through a tube to the localized volume between the skin and transducers (Fig. 1c, Supplementary Fig. 3a). To minimize signal background from blood and enhance detection of all iRBCs in the entire blood vessel cross-section, we developed an innovative array of 16 focused ultrasound transducers with semispherical sensitive surfaces in which the focal volumes were oriented in a line across the vessel along with a linear laser beam in the same orientation (Figs. 1a, 2b, Supplementary Fig. 3a–f). The acoustic focal points were also distributed at different depths to allow detection of iRBCs both in superficial capillaries (Fig. 2c, Supplementary Fig. 3b) and deeper (1–2 mm) and larger (1.0–1.5 mm in diameter) blood vessels (Fig. 2d, Supplementary Fig. 3b). To assist in the navigation of PA probe location, we also used near-infrared (NIR) imaging, followed by mapping the visualized blood vessels with white cosmetic markers transparent to the 1064 nm laser light (Fig. 2e–g, Supplementary Fig. 4a, b)⁴². All the components of this prototype, including the laser control box, AC/DC adapters, multichannel amplifier, and digitizer, were covered by plastic walls with metal film for electromagnetic shielding (Fig. 2a, Supplementary Fig. 3c).

Laser-induced PA signals from iRBCs have the typical bipolar waveform (Fig. 1b, top, in red), which are transformed (Supplementary Fig. 2) into unipolar transient peaks in the PA trace (Fig. 1b, bottom) with a width determined by time of flight of iRBCs through the detection volume. Due to the strong light scattering in the biotissue, which leads to blurring of the laser beam, the resolution of the Cytophone is

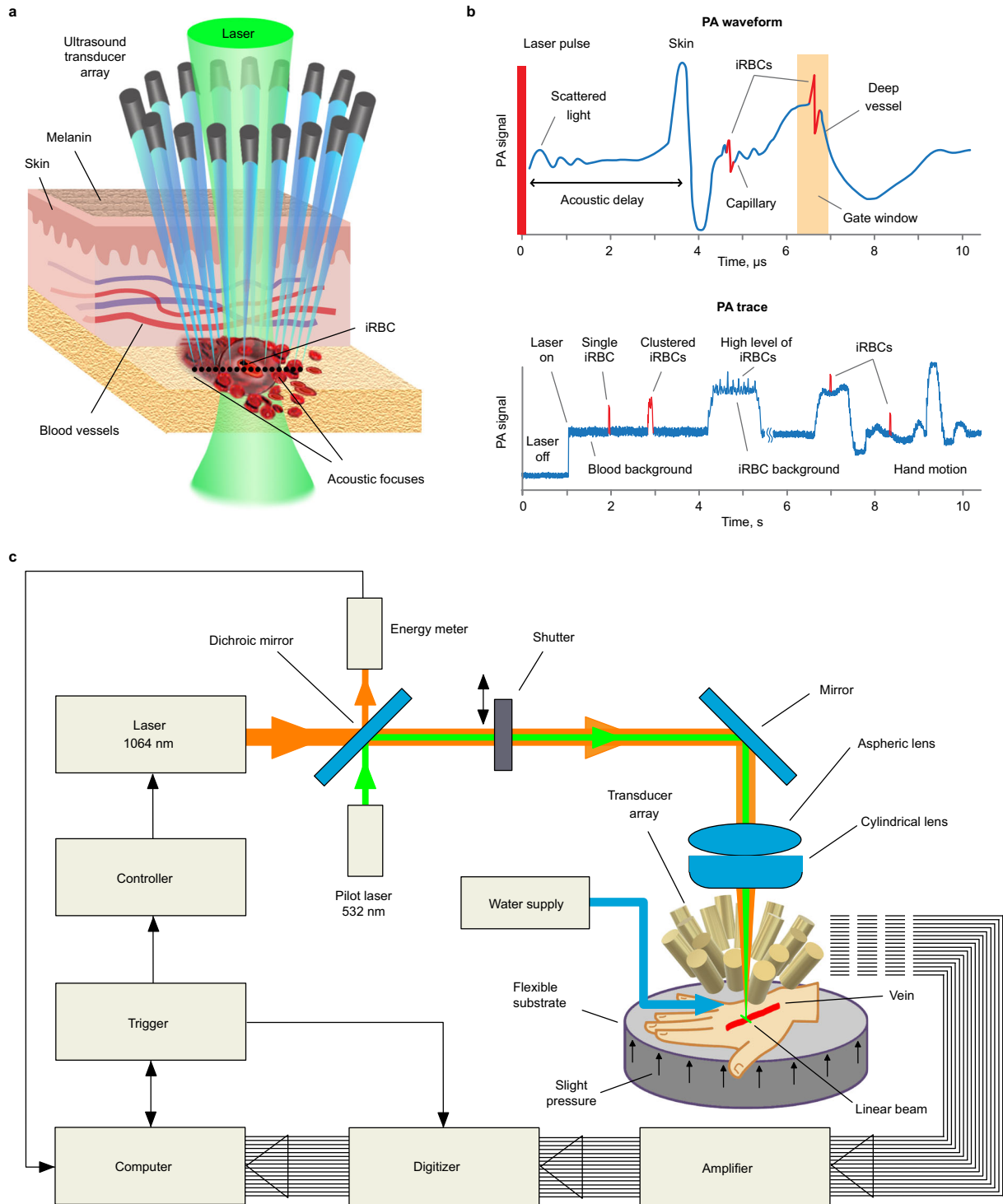


Fig. 1 | The principle of photoacoustic (PA) detection of circulating infected red blood cells in vivo with an acoustic resolution Cytophone. **a** Schematic of the focused ultrasound transducer array for assessing a blood network. **b** Typical PA signal waveform from iRBCs in superficial and deep vessels (top), and PA trace from single or clustered iRBCs with a high Hz absorption passing through the detection volume, resulting in a sharp positive transient PA peak above the blood background (bottom). **c** Schematic of Cytophone with the optical, multichannel acoustic, and electronic recording system. PA photoacoustic, iRBC malaria-infected red blood cell, μs microsecond, s second, nm nanometer.

determined by the acoustic resolution of focused transducers ($80 \pm 12 \mu\text{m}$)³⁴. The PA signals from many uninfected RBCs in the detection volume overlap and create a relatively stable blood background represented as the trace baseline (Fig. 1b, bottom). When single or clustered iRBCs with a high Hz absorption pass through the detection volume, local absorption increases resulting in a sharp positive transient PA peak above the blood background, (Fig. 1b). At high concentrations

and aggregated iRBCs at low and high concentrations in the blood background and motion artifacts (bottom).

In vitro validation of the Cytophone prototype using the blood vessel phantom

Initial validation of the Cytophone platform was performed in vitro using the same clinical PA setup, in which the human hand was

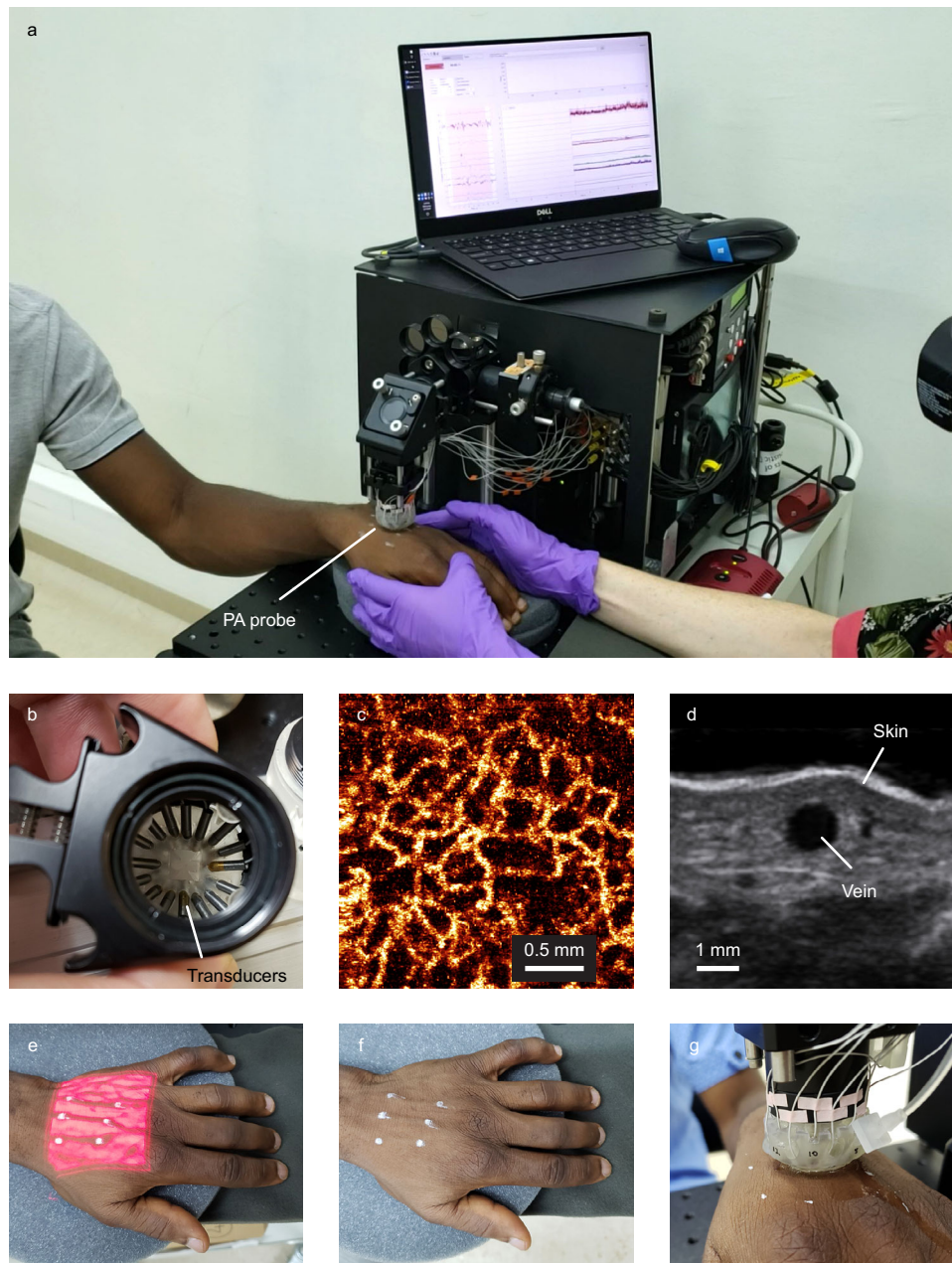


Fig. 2 | The Cytophone clinical prototype. **a** Photograph of the prototype during its alignment in a hospital in Yaoundé, Cameroon. **b** The focused ultrasound transducer array (top view). **c** Superficial vessel network in dorsal palm imaged with optical coherent tomography. **d** Ultrasound image of a vein in the dorsal palm. **e** Near-infrared (NIR) imaging with VeinViewer device of relatively large veins

mapped with white markers (stains) transparent to NIR laser radiation. **f** White marks indicate vein positions without NIR imaging. **g** PA probe consisting of an optical tip and the ultrasound transducer array adjusted to a marked vein. PA photoacoustic, mm millimeter.

replaced by a blood vessel phantom. The setup consists of a glass tube with a circular cross-section and inner diameter of 0.8 mm (Fig. 3a–c) with cell phantoms in static and dynamic conditions and a water tank for acoustic coupling^{38,41,43}. The use of this setup demonstrated the need to use contaminant-free water for acoustic coupling (Fig. 3d, Supplementary Note 1). The assessment of a commercially available Hz (tIrl-hz, InvivoGen, CA, USA) suspension in PBS flowing at 1 cm/s demonstrated excellent performance (Supplementary Note 1), displaying both PA waveforms (Fig. 3e) and PA traces (Fig. 3f), at expected vessel depths and Hz concentrations which are in the range for circulating human iRBCs (0.1–100 $\mu\text{g}/\text{mL}$) (Supplementary Fig. 5)^{23–26,37,39} In vitro testing of simple iRBCs phantoms (5.8 μm magnetic beads), which have NIR absorption spectra similar to Hz,

confirmed this conclusion (Supplementary Note 1, Supplementary Fig. 6)⁴³.

In vivo Cytophone device optimization in the training patient cohort

To optimize Cytophone performance and obtain initial safety estimation, we enrolled 11 adults and completed optimization in 10 adults with uncomplicated malaria (median 3300 parasites/ μL using varATS qPCR to quantify parasitemia). We tested the device at different settings, laser parameters, PA probe position and hand fixation. We also assessed levels of PA signals from the skin and vessels and compared PA signals from iRBCs and background. We noted that PA signals from skin areas above blood vessels were 1.5–2 times higher than from areas

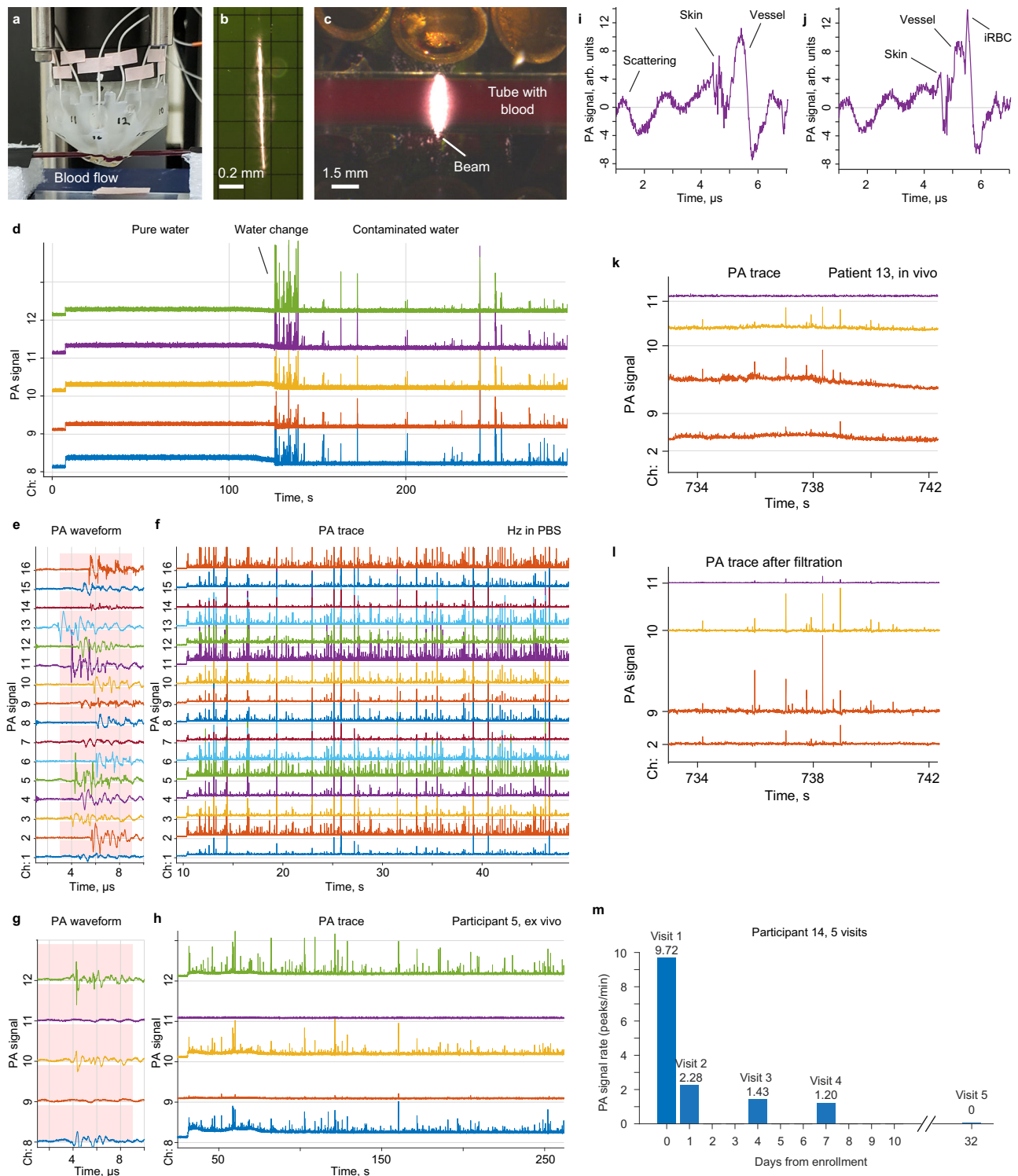


Fig. 3 | In vitro testing of Cytophone using vessel phantoms with cell phantoms, ex vivo testing of malaria-infected participant blood, and in vivo detection of iRBCs in infected participants in Cameroon. **a** Photograph of the PA probe consisting of an array with 16 transducers and an optical tip, and a simple vessel phantom consisting of a -1 mm diameter capillary tube with flowing blood. **b** Linear beam shape at a wavelength of 1064 nm after optical tip before passing through the vessel phantom. **c** Broadening of the linear laser beam after passing through the vessel phantom filled with blood. **d** PA signals from pure (left) and contaminated (right) water. **e, f** PA waveform (e) and PA trace (f) from 0.1 $\mu\text{g}/\text{mL}$ synthetic Hz suspension. **g, h** PA waveform (g) and representative PA trace (h) from

an unprocessed blood sample collected from an infected participant. Laser parameters: wavelength, 1064 nm, pulse width, 1.5 ns; pulse rate, 1 kHz; pulse energy, 130 μJ . **i, j** Typical PA signal waveforms in the dorsum of the hand illustrating before (i) and during (j) the passage of an iRBC through the detection point. **k, l** Typical PA traces from a malaria-infected participant before (k) and after (l) signal filtration. **m** Photoacoustic peak rates (peaks/min) from Participant 14 over multiple visits following antimalarial treatment. mm millimeter, arb. units arbitrary units, μs microsecond, s second, PA photoacoustic, min minute, Hz hemozoin, PBS phosphate-buffered saline, iRBC malaria-infected red blood cell. Source data are provided as a Source Data file.

without underlying vessels visible using ultrasound (Supplementary Fig. 7a), allowing us to navigate the PA probe without NIR imaging (Fig. 2e). We also observed complex PA waveforms with multiple patterns and time delays (Supplementary Note 2). These PA signal waveforms are then transformed into PA traces (Fig. 3k, l) where positive peaks have a width of 1–3 ms, which is associated with the time-of-flight of iRBCs through the detection volume. The true pulse PA signal waveforms from iRBCs have a specific bipolar shape, duration (0.2–0.4 μ s), and time delay (4.5–7 μ s) compared to the delay arising from background signals from the skin (2–3.5 μ s). These features allowed us to optimize software settings for time-resolved identification of signal origins, and the selection of true signals arising from iRBCs in the background of false signals. For instance, signal filtration and time gating provided a stable PA trace (Fig. 3k, l, Supplementary Fig. 8) due to effective removal of low-frequency motion-related fluctuation below 100 Hz (Supplementary Fig. 8) while retaining a much sharper true PA peak arising from iRBCs. Time gating also suppresses fluctuating background signals from pigmented skin (Supplementary Fig. 8).

Conventional POC diagnostic testing in the longitudinal cohort

We next began the longitudinal diagnostic performance study. Cameroonian adults ($n = 27$) presenting with uncomplicated malaria were tested at up to 5 visits over up to 37 days following treatment with a standard dose artemether-lumefantrine. Of the 27 participants enrolled, 20 contributed 94 total visits with PA trace and full diagnostic data for the final analyses, with 14/20 (70%) completing all 5 visits and 6/20 (30%) completing 4 visits (Supplementary Fig. 1). On visit 1 (Day 0; day of diagnosis and treatment), 18/20 of participants were smear-positive with a median parasite density of 1434 parasites/ μ L (IQR 129–4824), and 2/20 were RDT-positive/smear-negative (Table 1). Microscopy positivity rate and median parasite density both decreased over time (Table 1, Fig. 4). On day 0, of the 18 microscopy-positive samples, as determined by species-specific PCR⁴⁴, there were 16 *Pf* mono-infections, 1 *Pf/Pm* mixed-infection, and 1 *Pm* mono-infection; two samples were RDT-positive/microscopy-negative (Table 1). Over the full sampling period, 20/94 (21%) samples were microscopy-positive and 56/94 (60%) were RDT-positive.

Molecular quantification via qPCR and speciation via nested PCR in the longitudinal cohort

Using 10 replicates of a low concentration of cultured 3D7 ring-stage parasites and negative control samples, the limit of detection for the qPCR assay targeting *Pf*-specific varATS, as performed in our study, was 58.7 parasites/mL (Supplementary Fig. 9)⁴⁵. Nucleic acid was extracted from filter paper, and each qPCR sample was run in triplicate^{13,44,46}. On day 0, 19/20 (95%) of samples were *Pf*-positive (median density 1,280,623 parasites/mL (IQR 95,022–7,245,751)). The single-day 0 varATS-negative participant sample was *Pm*-positive by species-specific PCR⁴⁵. Both qPCR positivity rate and median density decreased over time with 4/19 participants qPCR-positive at the end of follow-up (Table 1, Fig. 4a, b). Overall, we detected *Pf* in 58/94 (62%) samples in our longitudinal cohort ($n = 20$ individuals) using varATS qPCR. Speciation was conducted targeting 18S small subunit ribosomal DNA⁴⁴. Of the nested PCR-positive samples, 40/47 (90%) were *Pf*-positive only, 3 were *Pf/Pm* mixed-infections, 1 was a *Pf/Po* mixed-infection, and 3 were *Pm* mono-infections (Table 1).

In vivo Cytophone diagnostic performance data

Cytophone (Supplementary Fig. 2) provides a count of PA peaks per unit of time, and data are presented as peaks per minute, referred to as the PA peak rate. We observed multiple peaks that exceeded the blood background at different rates and patterns (Supplementary Figs. 10, 11): (i) positive single peaks at a minimum width associated with individual iRBCs; (ii) positive peaks with relatively broader widths and

complex shapes associated with iRBC clusters; (iii) and wider peaks (>4 ms) with positive and negative components associated with artifacts (false positive signals). Median participant total testing time with Cytophone was 17 min per visit, however, some individuals were monitored for shorter or longer time periods (range 3–40 min). Although much shorter times (s) are required for PAFC-based detection of Hz, extended testing was conducted to adjust the probe location on the hand, optimize parameters, and gather additional data in our proof-of-concept study.

Analysis of the 94 traces identified PA signals from iRBCs with a specific bipolar (positive-negative) temporal shape, a time delay in PA waveform presentation, and positive peaks with a specific width in PA traces (Figs. 1b, 3i–j). By visit 3 (2–4 days following enrollment), the PA peak rate (peaks/min) declined or was 0 in 19/19 (100%) participants (Table 1, Fig. 3m, Supplementary Figs. 10, 11). On visits 1–5, 19/20 (95%), 9/16 (56%), 8/19 (42%), 4/20 (20%), and 1/19 (5%), respectively, had detectable PA signals (Table 1). Cytophone-positive samples had median PA peaks/min of 1.73 (interquartile range (IQR) 0.69–3.68), 1.63 (IQR 0.60–2.28), 1.18 (IQR 0.37–2.28), and 0.74 (IQR 0.26–1.47) on visits 1–4, respectively. One participant (ID # 31) had a positive PA signal on visit 5 (day 30).

When assessing the longitudinal trajectory of all participants together, the median PA peaks/min decreased by visit (Fig. 4a, b), as did the parasite density (Table 1, Fig. 4a, b). At the individual level, similar patterns of decreasing PA peaks/min were seen (Table 1, Fig. 4c, d, Supplementary Figs. 10, 11). However, there was no overall significant correlation between PA peak count and parasite density when looking at all concordant positive data points (Supplementary Fig. 12, Supplementary Table 2). Of note, microscopy and qPCR were not strongly correlated with a Pearson's correlation coefficient of 0.57 (Supplementary Fig. 13).

Performance of the Cytophone compared to microscopy and RDT

Using microscopy results to define disease status, Cytophone demonstrated 95% sensitivity at the time of enrollment and 90% sensitivity for all data points over longitudinal follow-up (Table 2). Cytophone and microscopy were both positive in 69 of 94 (73%) data points, with an additional 23 positive by Cytophone but negative by microscopy, and 2 data points negative by Cytophone but positive by microscopy. The receiver operator curve area under the curve (ROC-AUC) was 0.84 (95% CI 0.71–0.91), suggesting excellent diagnostic performance. (Table 2, Supplementary Fig. 14). Using RDT as the comparator, Cytophone and RDT were both positive for 71 of 94 (76%) samples, with 4 data points positive by Cytophone but negative by RDT and 19 data points negative by Cytophone but positive by RDT. The ROC-AUC was 0.79 (0.70–0.86), suggesting acceptable performance (Table 2, Supplementary Fig. 14). The single *Pm* mono-infection was successfully detected using Cytophone, microscopy, and RDT (Table 1).

Performance of the Cytophone compared to highly sensitive *P. falciparum* qPCR

Using highly sensitive qPCR as the gold standard, Cytophone correctly identified 61/94 (65%) samples, with 8 false positives and 25 false negatives. Cytophone had a sensitivity, specificity, positive predictive value (PPV), and negative predictive value (NPV) of 57% (95% CI 43–70), 78% (61–90), 80% (65–91), and 53% (39–67), respectively (Table 2). The AUC-ROC for Cytophone was 0.70 (0.60–0.78) (Table 2, Supplementary Fig. 14). The Youden index of Cytophone peaked at a varATS parasite density of ≥ 6 parasites/ μ L, indicating that the device was best able to detect true positives in samples with a density above this cut-off (Fig. 4e). In qPCR-positive samples above this cutoff, Cytophone had a sensitivity of 75% (95% CI 58–88). The Youden index optimal density cutoffs, based on varATS-derived densities, for nested PCR, microscopy, and RDT were ≥ 1 , ≥ 80 , and ≥ 5 parasites/ μ L, respectively (Fig. 4e).

Table 1 | Diagnostic results of (n = 20) participants included in the longitudinal study performance analysis

ID	Visit 1					Visit 2					Visit 3					Visit 4					Visit 5									
	Day	LM (p/mL)	varATS qPCR (p/mL)	RDT	Nested PCR	Cytophone (peak/min)	Day	LM (p/mL)	varATS qPCR (p/mL)	RDT	Nested PCR	Cytophone (peak/min)	Day	LM (p/mL)	varATS qPCR (p/mL)	RDT	Nested PCR	Cytophone (peak/min)	Day	LM (p/mL)	varATS qPCR (p/mL)	RDT	Nested PCR	Cytophone (peak/min)	Day	LM (p/mL)	varATS qPCR (p/mL)	RDT	Nested PCR	Cytophone (peak/min)
12*	0	9,831,000	2,416,331	H, L	Pf	13.52	3	4,360,000	2,321,588	H, L	Pf	7.90	7	0	551	H	Pf	2.28	32	0	0	H	-	0.00	32	0	0	H	-	0.00
13	0	1,181,000	4,400,994	H, L	Pf	17.69	4	0	0	H	-	1.44	7	0	0	H	-	0.00	29	0	218	-	-	0.00	29	0	218	-	-	0.00
14	0	4,098,000	25,925,074	H, L	Pf	9.72	4	0	0	H	-	1.43	7	0	0	H	-	1.20	32	0	0	-	-	0.00	32	0	0	-	-	0.00
15	0	139,000	162,724	H	Pf	3.35	2	0	134,006	H	Pf	0.00	7	0	0	-	-	0.00	30	0	0	-	-	0.00	30	0	0	-	-	0.00
16	0	122,000	80,116	H	Pf	2.53	2	0	10,760	H	Pf	0.00	5	0	8039	-	-	0.00	34	0	0	-	-	0.00	34	0	0	-	-	0.00
17	0	195,000	176,404	H, L	Pf	0.06	1	0	0	-	-	0.00	3	0	0	-	-	0.00	28	0	88	-	-	0.00	28	0	88	-	-	0.00
18	0	4,444,000	7,213,754	H, L	Pf	1.73	3	0	214	H	-	0.00	7	0	0	H	-	0.00	30	0	0	-	-	0.00	30	0	0	-	-	0.00
19	0	23,529,000	29,462,941	H, L	Pf	1.53	2	0	57,798	H, L	Pf	0.83	9	0	1147	H	-	0.00	36	0	0	-	-	0.00	36	0	0	-	-	0.00
21	0	24,000,000	83,840,574	H, L	Pf	1.02	3	0	45,696	H	Pf	0.00	6	0	1067	H	Pf	0.00	31	0	0	-	-	0.00	31	0	0	-	-	0.00
22*	0	131,000	248,059	H, L	Pf, Pm	2.15	4	0	1401	-	Pm	0.00	11	0	0	-	-	0.00	30	0	0	-	-	0.00	30	0	0	-	-	0.00
23*	0	60,546,000	23,889,209	H, L	Pf	4.00	1	0	23,902,338	H, L	Pf	4.29	7	0	154	H	-	0.00	29	0	0	-	-	0.00	29	0	0	-	-	0.00
24	0	0	43,637	H	Pf	7.56	2	0	963	-	-	0.00	2	0	1416	-	-	4.82	6	0	742	-	-	0.00	29	0	2,884,435	-	-	0.00
26	0	1,200,000	196,075	H	Pf	0.00	4	0	2204	-	Pf	0.00	4	0	0	-	-	0.00	35	0	0	-	-	0.00	35	0	0	-	-	0.00
27	0	3,578,000	0	L	Pm	0.54	3	0	0	L	Pm	1.63	7	0	0	-	-	0.00	30	0	0	-	-	0.00	30	0	0	-	-	0.00
28*	0	5,964,000	2,630,750	H, L	Pf	0.85	3	0	738	-	Pf	0.00	7	0	195	-	-	0.00	30	0	0	-	-	0.00	30	0	0	-	-	0.00
29*	0	68,000	7352	H	Pf	0.36	2	0	0	H	-	0.00	6	0	0	H	-	0.00	34	0	0	-	-	0.00	34	0	0	-	-	0.00
30*	0	1,667,000	99,991	H	Pf	0.47	2	0	471	H	-	0.14	7	0	0	H	-	0.00	29	0	0	-	-	0.00	29	0	0	-	-	0.00
31*	0	2,908,000	7,341,742	H, L	Pf	1.16	2	0	702	H	Pf	0.36	7	0	0	H	-	0.28	30	0	0	-	-	0.28	30	0	0	-	-	0.28
32	0	0	6,143	H	Pf, Po	0.51	1	0	138	-	-	0.16	5	0	0	-	-	0.00	30	0	526	-	-	0.00	30	0	526	-	-	0.00
33	0	42,000	2,313,187	H	Pf	1.86	2	0	4883	H	Pf	0.00	7	0	0	H	-	0.37	29	0	0	-	-	0.00	29	0	0	-	-	0.00

n number, LM light microscopy, ID study identification number, p parasites, varATS var gene acidic terminal sequence, qPCR quantitative polymerase chain reaction, PCR polymerase chain reaction, RDT rapid diagnostic test, H antigen histidine-rich protein 2 positive, L parasite lactate dehydrogenase positive, Pf Plasmodium falciparum positive, Pm Plasmodium malariae positive, Po Plasmodium ovale positive.

*Missing visit due to scheduling conflict.

†This individual took 2 doses of malaria medication within 12 h of study enrollment.

‡Missing visit due to technical difficulties.

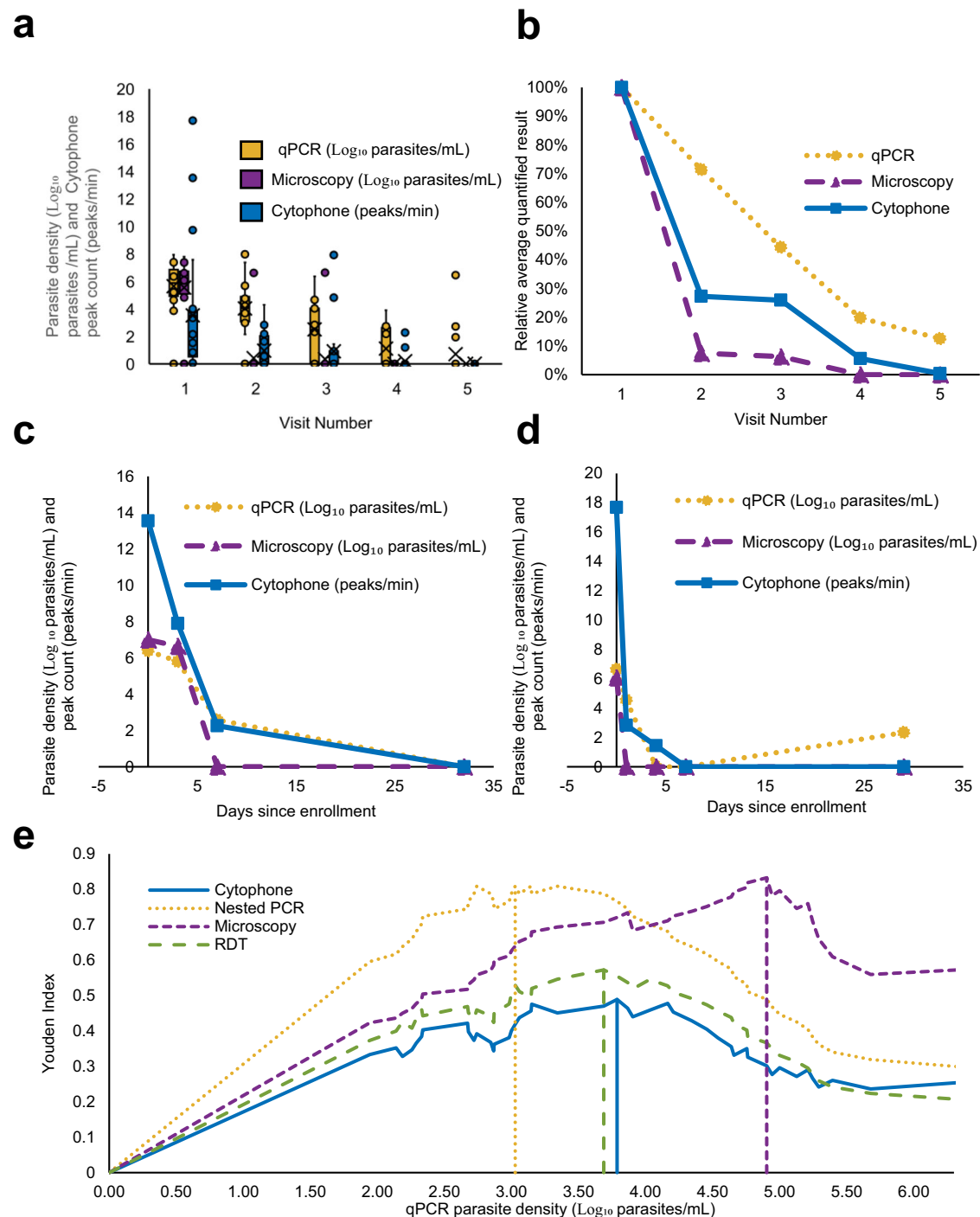


Fig. 4 | Quantitative result trends and optimal detection thresholds. **a** Box and whisker plot of $n = 94$ quantitative results for parasite density and photoacoustic signals by study visit. In this plot, individual data points are shown as circles. The box represents the interquartile range (25th to the 75th percentile) of data, and the line through the box shows the median (50th percentile). The whiskers on the ends of the box show the 5th and 95th percentiles of data points, and the x represents the mean. Data presented represents individual measurements for $n = 20, 16, 19, 20,$ and 19 participants on Visits 1–5, respectively. **b** plot of the average quantitative result for parasite density and photoacoustic signals ($n = 94$) by study visit relative

to results at enrollment on visit 1, day 0. **c, d** line plots of quantitative diagnostic results by days since enrollment for participants 12 and 13, respectively. **e** plot of the Youden index value by qPCR parasite density for Cytophone, nested PCR, microscopy and RDT created using diagnostic results from $n = 94$ participant visits. The Peak Youden index value, indicating the optimal cutoff for the detection of a positive sample, is indicated by a vertical line for each diagnostic. qPCR quantitative polymerase chain reaction, RDT rapid diagnostic test. Source data are provided as a Source Data file.

Safety and acceptability of in vivo Cytophone assessment

A similar version of the Cytophone device used in an NIH-sponsored human trial for melanoma has shown an excellent safety profile and has been deemed a non-significant risk (NSR) device by the United States Food and Drug Administration (FDA). Potential risks of

Cytophone assessment are local skin irritation, burning sensation, and eye injury. To mitigate risks to the skin, study clinicians carefully monitored the assessment area for any indication of irritation or burning. If any such adverse reactions were reported, the procedure was aborted, and local treatment was provided. To minimize the risk of

Table 2 | Comparative performance of the Cytophone and conventional diagnostics used in the study

Characteristic	qPCR as reference				Nested PCR as reference			Microscopy as reference		RDT as reference
	Nested PCR	Microscopy	RDT	Cytophone	Microscopy	RDT	Cytophone	RDT	Cytophone	Cytophone
<i>Results, n</i>										
True positive	43	19	43	33	20	41	31	20	18	37
False positive	4	1	13	8	0	15	10	36	23	4
True negative	32	35	23	28	47	32	37	38	51	34
False-negative	15	39	15	25	27	6	16	0	2	19
<i>Performance characteristics, % (95% CI)^a</i>										
Sensitivity	74 (61–85)	33 (21–46)	74 (61–85)	57 (43–70)	43 (28–58)	87 (74–95)	66 (51–79)	100 (83–100)	90 (68–99)	66 (52–78)
Specificity	89 (74–97)	97 (85–100)	64 (46–79)	78 (61–90)	100 (92–100)	68 (53–81)	79 (64–89)	51 (39–63)	69 (57–79)	89 (75–97)
Positive predictive value	91 (80–98)	95 (75–100)	77 (64–87)	80 (65–91)	100 (83–100)	73 (60–84)	76 (60–88)	36 (23–50)	44 (28–60)	90 (77–97)
Negative predictive value	68 (53–81)	47 (36–59)	61 (43–76)	53 (39–67)	64 (52–74)	84 (69–94)	70 (56–82)	100 (91–100)	96 (87–100)	64 (50–77)
Accuracy	80 (70–87)	57 (47–68)	70 (60–79)	65 (54–74)	71 (61–80)	78 (68–86)	72 (62–81)	62 (51–72)	73 (63–82)	76 (66–84)
ROC curve AUC	0.82 (0.72–0.88)	0.65 (0.58–0.71)	0.69 (0.58–0.78)	0.70 (0.60–0.78)	0.71 (0.63–0.78)	0.78 (0.68–0.85)	0.76 (0.66–0.84)	0.76 (0.69–0.81)	0.84 (0.71–0.91)	0.79 (0.70–0.86)
AUC comparison (p-value) ^b	0.02	0.26	0.85	Ref	0.30	0.74	Ref	0.12	Ref	–

qPCR quantitative polymerase chain reaction, PCR polymerase chain reaction, RDT rapid diagnostic test, n number, CI confidence interval, ROC receiver operating characteristic, AUC area under the curve, ref reference for comparison.

^aThe 95% CIs were calculated using the exact binomial method.

^bThe p-value is the probability that the true AUC (ref) equals the AUC (comparison), given the sample data.

eye injury resulting from the laser being directed at the eye, protective goggles were provided and the laser was mounted in place to avoid any undesired movement.

In this study, we found that Cytophone assessment was safe, with only one participant among 37 reporting an adverse event (AE) over the study period. The single reported AE, a moderate severity skin lesion in an area of the body not tested with Cytophone, was deemed to be a dermatological reaction to the antimalarial and unrelated to the device. The AE lasted three days, self-resolved, and the subject continued in the study with no further AEs reported. Following PAFC testing, no acceptability issues were reported post-procedure by study participants via questionnaire.

Discussion

This report demonstrates the successful application of the PAFC-based Cytophone with a focused ultrasound transducer array and a linear thermoacoustic signal generation for the *in vivo* identification of hemozoin as an effective malaria diagnostic test in humans with uncomplicated malaria. Despite significant progress in *in vivo* diagnostic techniques, including bright-field, fluorescence, and PA imaging, no clinically relevant methods have been developed that are able to noninvasively and rapidly detect fast-moving iRBCs in the human bloodstream with high sensitivity^{17–30}. The noninvasive and safe Cytophone device demonstrated $\geq 90\%$ sensitivity and overall excellent diagnostic performance compared to invasive POC microscopy-based detection and approached the diagnostic performance of standard PCR, with the potential for further Cytophone advances. Our study was conducted on-site at a hospital clinic in Yaoundé, Cameroon, demonstrating the ability of the device to be used in an endemic setting. Initial testing was conducted jointly between the US and Cameroonian teams, but due to COVID restrictions, the majority of testing was conducted by trained Cameroonian staff. Training for ~4–6 h was required for staff to successfully operate and acquire data, with an additional few days to gain experience with optimizing probe placement. The current trial was built on the results of extensive technology

development, *in vitro* and *in vivo* murine studies using linear and nonlinear nanobubble-based PAFC technology since 2006, with an initial focus on diagnosing cancer^{34,35,37–39,47}. Building on the similarity in PA properties of melanin and Hz, we explored the potential for PAFC to detect iRBCs based on the presence of intraerythrocytic strongly light-absorbing Hz^{37,39}. Notably, our prototype device was tested in Cameroonian adults, all with dark skin and high melanin content. PA interference from melanin was avoided using time-resolved detection and differentiation of the readily distinguishable time delays between the signals from the skin and the signals from iRBCs in vessels (Figs. 1b and 3j). Cytophone has the potential to be a breakthrough device allowing for noninvasive (no blood draw needed), rapid (seconds to minutes), label-free (no contrast agent needed), and safe (no skin damage, pain, or blood contamination) *in vivo* diagnosis of malaria.

The WHO seeks to reduce malaria case incidence by at least 90% globally and to eliminate malaria from 35 countries by 2030, as compared to 2015¹. The lack of an optimal POC diagnostic is a major obstacle to reaching these goals. Major challenges relate to insufficient sensitivity to detect the asymptomatic reservoir or low-density infections, the inability to reliably detect all human species, and specific to RDTs, a susceptibility to target antigen deletions and persistence of circulating antigens^{4,10,48,49}. Our longitudinal study design allowed us to assess *Pf* parasite burdens ranging from 88 to 90,777,944 parasites/mL (-0.000002 –1.8% parasitemia), typical densities for uncomplicated malaria in most settings. PA signals were detected in 19 of 20 participants at the time of presentation with malaria, and parasitemia in the single Cytophone-negative individual was 196 parasites/ μ L. Following treatment, PA signals showed a consistent downward trend similar to the trajectory of qPCR and POC results, with significant decreases over the initial 3–5 days following antimalarial therapy (Fig. 4, Supplementary Figs. 10, 11). By days 7–11, RDTs remained positive in 50% of adults, which is likely due to HRP-2 antigen persistence following treatment. Over this same time span, Cytophone was positive in only 20% of participants, suggesting that PAFC may be less prone to this issue than HRP-2-based RDTs⁴⁹. It is also anticipated that Cytophone

performance will not be adversely impacted by *P. falciparum* parasites with HRP-2 deletions, a significant additional threat to current RDTs'. At the end of follow-up, between days 28 and 36, one adult had a detectable PA signal but negative RDT, varATS qPCR, and nested PCR. Whether this represents a recurrent infection, the presence of residual Hz (e.g. intraleukocytic), or a false positive is unclear and will require further study in a larger longitudinal dataset and in those with lower parasite densities. Compared to molecular methods, the AUC-ROCs of the Cytophone, microscopy, or RDT were not significantly different from one another. Thus, our prototype in a field-based initial human study has demonstrated comparable noninvasive Cytophone diagnostic performance to currently utilized invasive POC malaria diagnostics, a major advancement in the malaria diagnostic field.

An additional promise of the Cytophone is the anticipated ability of the device to detect all species of *Plasmodium*, as the production of Hz is central to *Plasmodium* survival within the iRBC⁴⁹. Reports by our group and others have clearly documented poor RDT performance for detecting non-*falciparum* species^{6,48}. As *Po*, *Pm*, and *Pv* are increasingly reported in sub-Saharan Africa, universal diagnostics are desperately needed^{3,6,50}. In our pilot study, one adult with a non-*falciparum* mono-infection (*P. malariae*) was successfully detected by Cytophone, and two adults with mixed infections (*Pf* plus a non-*falciparum* species) were also detected.

Our in vivo diagnostic device success was enabled by the integration of several technological innovations in into our portable Cytophone design, not present in our earlier in vitro and in vivo murine malaria studies using a relatively larger non-portable prototype³⁷. Notable innovations include: (1) the use of a compact high-pulse-rate repetition solid crystal laser, (2) a unique ultrasound transducer, (3) high-speed signal processing using time-resolved gating of PA signals in a waveform window, and (4) filtering of sharp iRBC-related peaks in PA traces (Fig. 1b). Our linear laser beam and linearly distributed acoustic foci with lengths which exceed the vessel diameter (Fig. 1a, c) allow PA data to be tolerant to horizontal PA probe positioning (along skin surface). The multi-focused transducer array with different focal lengths (Supplementary Fig. 3b) enables PA data to be tolerant to vertical probe positioning and allows for the simultaneous detection of iRBCs at depths from superficial capillaries to 5–10 mm deep veins and arteries (Supplementary Fig. 5). Time-resolved gating allows signal capture from iRBCs arriving at a distinguished time delay compared to the background signals from pigmented skin, hairs, and scattering light. Unlike our previous melanoma study, which used a fixed holder for hand stabilization³⁸, the current prototype design allowed hands to remain free during assessment (Fig. 2a). Our software enables us to filter low-frequency motion artifacts while retaining the sharp PA peaks from fast-moving cells (Fig. 3k, l), making Cytophone tolerant to natural hand motions and reducing the need for time-consuming PA probe navigation. Additionally, a crucial advantage of Cytophone is that iRBC concentration is related to PA signal rate (i.e., peak numbers from iRBCs in PA traces) and not to signal amplitude. Thus, quantitative data on iRBCs does not depend strictly on the laser energy and/or absorption of Hz; both have to be sufficient to create countable PA signals with a signal-to-noise ratio (SNR) of $\geq 2-3$.

The success of our prototype in this trial is encouraging. We anticipate significant improvements in the SNR and detection limit will be possible with the use of shorter laser pulses (e.g., 100 ps vs. 1.5 ns) which should enhance sensitivity by at least 10 \times due to more effective generation of PA signals arising from smaller (50–100 nm) Hz crystals. Based on prior³⁸ and current data (e.g., 5–15 PA signals detected during several second windows) (Fig. 3l), we estimate that with 10 s of dorsal hand vessel testing, we can assess approximately 0.2–2.0 mL of blood (given a typical flow rate range of 0.02–0.2 mL/s)^{38,39}, dramatically higher than the 5–10 μ L of blood collected with current POC diagnostics. Assuming the presence and ability to detect at least one Hz-containing RBC in 1 mL of blood, the theoretical detection limit

(Supplementary Discussion) would be significantly better than available methods, and detection could occur in well under one minute.

Testing of both malaria-uninfected individuals in endemic areas and the characterization of signals arising from free Hz or intraleukocytic Hz⁵¹ in vivo in humans is underway and will allow further refinements in Cytophone's capabilities. Due to the differences in light absorption between plasma, RBCs, and leukocytes, we anticipate that the Cytophone will be able to distinguish between these potential sources of Hz⁴¹. The ability of Cytophone to quantify parasitemia will also be critical. In our current study, we did not assess vessel diameter and flow rate, which is needed to approximate the volume assessed per unit time, and thereby calculate approximate parasite density. In our previous melanoma study, we were able to assess approximately 1 L of blood in 10–15 min through Cytophone measurements on the cubital vein [diameter, 3–4 mm; flow velocity, 7–8 cm/s (flow rate -1.3 mL/s)³⁸. We do not expect that vessel size will impact Cytophone performance, however, we will conduct vessel diameter and flow rate measurements in future studies to additionally facilitate interparticipant comparisons and assess device performance in pediatric subjects. Although analytical variability (repeated measurements within a short period of time in the same individual) was not assessed in this study, reproducibility has been assessed in a vessel phantom with PA signal amplitude fluctuation of 19–26%, which is typical for PA techniques^{38,43,52}. Finally, further work is underway to assess the ability to both detect and distinguish all human malaria species. Based on our prior in vivo murine studies, we anticipate that this will be feasible due to differences based on the size and shape of Hz crystals, iRBC size (reticulocyte versus normocyte), possible tiny spectral Hz fingerprints, and circulating parasite life cycle stages, whose Hz contents is expected to differ between species^{41,53}. Variations in Hz crystal size, shape, and distribution will also contribute to the Cytophone's ability to distinguish between ring-stage parasites, circulating gametocytes, and sequestered trophozoites.

Our initial PAFC clinical devices were constructed for feasibility studies and were built as stationary laboratory setups using relatively large, expensive solid lasers^{37–39}. Recent advances in laser technology have made it possible to use compact, cost-effective solid lasers for building the tabletop Cytophone prototype used in the current study and we anticipate using laser diodes in the future⁴¹. Although exact cost estimates are not available at this stage of development, the minimal use of consumables, the increasing affordability of laser technology, and the long lifespan of lasers (up to 7 years) compared to the short time needed for Hz detection (<1 min), indicate that the potential cost per malaria diagnosis for the Cytophone is low. We expect that tabletop Cytophones could be used in malaria endemic 2nd tier clinics/hospitals and referral hospitals. In addition, devices could be considered in elimination areas, as it would allow rapid screening at checkpoints. Cytophone also constitutes a promising research tool to study in vivo disease dynamics, pathophysiology, and the efficacy of new drugs and vaccines by assessing iRBCs in vivo before and after treatment, particularly for drugs that act on the hemoglobin digestion pathway, studies which have hitherto been unachievable. Finally, pilot data suggest that PAFC may be able to detect sickle cells⁵⁴. The ability to detect sickle cells and iRBCs non-invasively would be a major diagnostic advancement in sub-Saharan Africa, where both diseases are co-endemic.

In conclusion, we believe that our longitudinal data in Cameroonian adults with symptomatic malaria clearly demonstrate the ability to noninvasively detect iRBCs, a major advance in the malaria diagnostic landscape. Our clinical Cytophone prototype for malaria was safe, necessitated a short training time to collect data, and diagnostic performance was already comparable to current standard POC tests, with significant room for further prototype enhancements. Assessment of the next generation of Cytophone prototypes is ongoing and will provide further information concerning analytical

variability, reproducibility, and diagnostic performance in an expanded study population, including individuals with undifferentiated fever, asymptotically infected individuals, and malaria-uninfected individuals from nonendemic settings.

Methods

Study site and ethical considerations

This study complied with all relevant ethical regulations and was approved by the Yale Human Investigations Committee, National D'Éthique De La Recherche Pour La Sante Humane in Cameroon, and The Centre Hospitalier et Universitaire de Yaoundé. Informed consent was obtained for every participant enrolled in the study and compensation was given at each visit. Our study was conducted in Yaoundé, the capital of Cameroon, with a population of 3 million inhabitants. Malaria is holoendemic with two distinct rainy seasons and a wide range of entomological inoculation rates (0–90.0 infective bites per person per year)⁵⁵. The Yale, UAMS and Cameroonian teams were onsite in February 2020, with the UAMS team supervising the technical aspects of the device and the Yale and Cameroonian teams responsible for all clinical and molecular protocol aspects. Due to the COVID-19 pandemic travel restrictions, US-based teams had to leave Cameroon in March 2020, while a local Cameroonian team member was trained on how to acquire data with the Cytophone, and enrollment and follow-up under COVID-19 guidelines were continued for the duration of the study.

Regulatory approvals and study site setup

This research study was initiated under a Research Collaboration Agreement (Memorandum of Understanding) between the University of Arkansas for Medical Sciences and the Yale School of Public Health (YSPH) in 2019. The Yale Human Investigations Committee (HIC) determined Cytophone to be an NSR device with abbreviated Investigational Device Exemption (IDE) requirements under the FDA Code of Federal Regulations Title 21 812.2. Yale HIC approved the clinical protocol, followed by approval at the National D'Éthique De La Recherche Pour La Sante Humane in Cameroon (CNERSH) and The Centre Hospitalier et Universitaire de Yaoundé (CHUY). The Cytophone was then shipped from YSPH to Médecins Sans Frontières (Doctors without Borders) Epicentre (MSF Epicentre) in Yaoundé, Cameroon, under a Material Transfer Agreement in January 2020. The study device was set up in a dedicated study room on the medical campus of CHUY, the University Teaching Hospital of Yaoundé.

The Yale, UAMS, and Epicentre teams were present for the device set up in February 2020, with the UAMS team supervising technical aspects of the Cytophone device, including calibration within the dedicated room, and the Yale and Cameroonian responsible for all other protocol aspects, including participant recruitment, clinical management, follow-up, and testing, as well as laboratory assays. While it was the intent for Yale personnel to remain on hand for the entirety of patient recruitment, the COVID-19 pandemic necessitated that a local Cameroonian team member be trained in the use of the Cytophone. We estimate that a total of ~4–5 h was sufficient for initial training to use the Cytophone. However, further training is needed to understand the theory of operation and to perform data analysis. Due to COVID-19 travel restrictions, all international teams left Cameroon in March 2020, and locally trained staff continued enrollment and follow-up under COVID-19 infection control and prevention guidelines, alongside daily email/phone communications and weekly multi-site teleconferences (e.g., Zoom® meetings) throughout study participant involvement.

Participant recruitment and clinical follow-up

Our study was conducted in two consecutive phases: (1) a training cohort assessed at a single visit for initial device optimization and safety assessments and (2) a separate longitudinal study cohort seen

for up to 5 visits spanning up to 37 days to assess diagnostic performance and safety (Supplementary Fig. 1). All participants were adults presenting with uncomplicated malaria. The longitudinal cohort was seen on days 0 (the day of diagnosis and start of treatment), 1, 3 [± 1 day], 7 [± 3 days], and 30 [± 7 days]. A goal of this longitudinal design was to provide samples with declining parasite densities and complete clearance (negative samples), as it was anticipated that quantitative PCR (qPCR) would be negative by day 30 in nearly all participants, with low probability of reinfection in this setting. Inclusion criteria for both cohorts were the following: adults age ≥ 21 years with uncomplicated malaria confirmed by either RDT or blood smear microscopy, willingness to adhere to the protocol, and residence in Yaoundé. Exclusion criteria included the following: diagnosis of severe malaria, a history of severe mental illness, presence of known hemoglobinopathies, cancer undergoing active treatment, pregnant (pregnancy testing done at enrollment) or breastfeeding women, and recent receipt of anti-malarial therapy within 2 weeks to 12 h of enrollment. Although children, pregnant, and breastfeeding women have the greatest risk of malaria-related morbidity and mortality, they were excluded from this study because of the need to conduct an initial safety assessment of the device before expanding to include more populations. There were no exclusion criteria in this study based on sex, although pregnant and breastfeeding individuals were excluded because of the novel, first-in-human assessment of our technology because of the increased vulnerabilities of those groups. Sex was self-reported by participants, and gender was not considered in the study design. Sex- and gender-based analyses were not performed in this study given that we did not expect sex or gender to have an impact on the diagnostic performance of our device. Study staff recruited participants from the University Teaching Hospital of Yaoundé or nearby clinics. Following informed consent, a brief questionnaire and clinical exam were conducted to obtain details on patient demographics and clinical presentation. Upon confirmation of malaria diagnosis, participants were provided artemether-lumefantrine taken orally twice a day for 3 days, following Cameroonian and international guidelines⁵⁶. At each visit, we performed Cytophone assessment and collected venous blood (5 mL in EDTA tubes) for thick and thin smears, an RDT, and storage on Whatman® FTA® Cards (MilliporeSigma, Inc.).

PAFC-based Cytophone device

The Cytophone for malaria prototype (Figs. 1 and 2) was built using a near-infrared (NIR) laser (Wedge HB, Bright Solutions, Caru Carpignano, Italy) with the following parameters: wavelength, 1064 nm; pulse width, 1.5 ns; pulse repetition rate, 1–2 kHz; and pulse energy on the skin, 240 μ J. For navigation and visualization, a low-power continuous-wave laser (532 nm, 4.5 mW, model CPS532, Thorlabs, Inc.) was adjusted collinearly with the NIR laser beam with dichroic mirrors (Di02-R561; Semrock). A linear laser beam with dimensions of $11 \times 1500 \mu$ m was formed by assembling aspheric (C560TME-C) and cylindrical (LJ19181I-C) lenses (Thorlabs Inc.) having an antireflection coating and a focal distance of 12.7 mm. During the course of the study, trained staff performed periodic laser alignment control with a built-in CCD camera (DCC1645C; Thorlabs). Additionally, real-time laser energy with a USB-based energy meter was monitored (PM100USB, S314C head; Thorlabs).

To improve the signal-to-noise (blood background) ratio (SNR), we developed an innovative ultrasound transducer array with 16 customized focused spherical transducers with the following parameters: diameter, 2.4 mm; focal lengths, 3–7 mm; frequency, 40–50 MHz; and resolution, 70–90 μ m. The 16-transducer array provides a range of acoustic focal spot positioning, at 0.5, 1.0, 1.5, 2.0, and 2.5 mm depths below the skin surface, in clusters of 3, 4, 3, 3, and 3 transducers, respectively, enabling detection of iRBCs at different vessel locations. The transducers were fixed into a customized holder that was built using a high-resolution stereolithography 3D printer (Form 2,

Formlabs, Inc.). Water was used for acoustic coupling between the transducers and the participant's skin. Within the transducer holder, a 3 × 5-mm central oval was present for laser beam propagation, and two small holes were used for water delivery and suctioning (Supplementary Fig. 3a).

A 16-channel amplifier (Flash Amp, PhotoSound Inc., Houston, TX, USA) was used to amplify PA signals from the transducer array. The PA signal acquisition system for the Cytophone device consisted of a data acquisition board (ATS9416, AlazarTech), a laptop computer (XPS 13, Dell), and a pulse generator (Sapphire 9200, Quantum Composers Inc., Bozeman, MT, USA). The acquisition board was housed in a PCIe card expansion system (Echo Express SE I, Sonnet Technologies, Irvine, CA). We developed The Cytophone software in MATLAB v.9.2 (The MathWorks, Inc.). The laser was triggered at 1 kHz and the pulse generator provided synchronization between laser pulses and data acquisition.

PA signal sampling and processing

The Cytophone device sampled PA signals at a rate of 100 MHz. To increase the SNR, we averaged four consecutive PA signal waveforms. These signal waveforms were then transformed into PA traces using their peak-to-peak amplitudes, similar to those produced in standard flow cytometry³². The PA trace baseline corresponded to background signals from uninfected RBCs. When iRBCs containing the target Hz pass through the area of the vessel under assessment by the Cytophone device, they absorb more laser energy and produce a stronger PA signal which appears as a positive peak above the uninfected RBC blood background trace. The widths of these PA peaks correspond to the time-of-flight of the iRBCs through the detection volume.

We eliminated background fluctuations using a high-pass filter (10 Hz cutoff frequency) before peak detection. The threshold for peak detection was determined using the equation $PA_{th} = m + k \cdot IQR$, where m is the median, IQR is the interquartile range of the trace, and k is a constant determined from control experiments. The envelope of background signals in the PA trace varies depending on the blood vessel size and other factors (e.g., skin pigmentation, hairs, hand movements, flow dynamics, and laser energy fluctuations) during in vivo measurements. To reduce the influence of these factors, we programmed the software to analyze the PA trace in 10-second-long windows, and PA data were recalculated in each window. Once the software identifies PA peaks, it measures peak properties such as normalized amplitude and full width at half maximum. During post-processing, we manually checked the trace for artifacts and visualized the PA signal. Signal shape, width, and time delay-related selection criteria were used to identify and exclude any artifact-associated PA peaks.

In vitro and in vivo Cytophone assessment

Initial Cytophone assessments were performed in vitro using vessel and cell phantoms to establish fluctuations in the PA trace baseline caused by electronic noise, the influence of scattered light, instability of the laser energy, acoustic environmental noise, vibration, and sample motion. For Cytophone in vivo testing, hand images were taken in the area where the device was focused before and after assessment for grading of local skin pigmentation using a system with three simplified categories: dark, medium, or light. While seated, the participant placed their hand on a flexible foam substrate beneath the PA probe. The participant's hand was adjusted until the selected vessel was directly below the PA probe, and the probe was then lowered until it made contact with the interface of contaminant-free water for acoustic coupling. Participants could request that the Cytophone assessment stop at any point. We considered a PA contrast usable for navigation and detection of Hz if the PA signal from the vessel was above the established noise threshold and more than 1.3–1.5-fold higher than the PA signal from surrounding skin tissue. NIR imaging (AV300M, AccuVein Inc., Palatine, IL, USA) was also used for vessel visualization. The

median duration of trace time analyzed per visit for an individual participant was 14 min (range 2–24 min). Cytophone data analysis was performed by the UAMS software specialist.

Conventional malaria diagnostics

Thick and thin blood smears were stained using 10% Giemsa for 15 min. All blood smears were read independently by two trained microscopists, one of whom is a WHO level 2 certified microscopist. Study microscopists calculated parasite densities from thick blood smears by counting the number of asexual parasites per 500 leukocytes, assuming a leukocyte count of 8000/μL, providing a detection limit of 16 parasites/μL. We declared a sample negative (below the limit of microscopic detection) when no asexual parasites were seen after counting 500 WBCs. A third microscopist read any discrepant speciation or quantitative results if a >25% difference between the two readings was noted; we reported concordant species and median quantitative values. All participants were tested at each visit with a CareStart™ Malaria Ag Pf/Pan COMBO RDT (catalog #RMRM-02571; WHO-prequalified histidine-rich protein 2/lactate dehydrogenase RDT) per manufacturer's instructions.

Molecular diagnostics

Blood samples were shipped from Cameroon to YSPH on dry ice in March 2021. To extract nucleic acid from the samples, 6 mm hole punches of filter paper from each sampling point were placed in individual Eppendorf tubes with 1 mL of 10% saponin in PBS (phosphate buffered saline) and stored overnight at 4 degrees Celsius⁴⁶. After rinsing in PBS, the samples were incubated for 10 min in a heat block at 95 °C in 1 mL of Chelex 100 (Bio-Rad Laboratories, Inc.), and the supernatant of spun-down tubes contained the extracted DNA used in our study⁴⁶. *Plasmodium falciparum* positive controls were derived from cultured 3D7 parasites, and negative controls were derived from blank filter paper. A standard curve was created using samples ranging from 10% to 0.000001% parasitemia (500,000 parasites/μL to 50 parasites/mL) for each qPCR run of sorbitol-synchronized ring-stage 3D7 parasites serially diluted in whole blood, run in duplicate (Supplementary Fig. 9)⁵⁷. For highly sensitive parasite detection, we conducted qPCR targeting the var gene acidic terminal sequence (varATS, 59 copies/genome) which has a published LoD of 60–150 parasites/mL for ring-stage cultured 3D7 parasites¹³. For speciation, an initial round of *Plasmodium* genus-specific PCR was accomplished using the following primers, rPLU 6 TTAAATG-CAGTTAAAACG and rPLU 5 CCTGTTGTTGCCTTAAACTTC⁴⁴. This was followed by nested species-specific PCR targeting 18S small subunit ribosomal DNA, conducted in duplicate⁴⁴. The species-specific primers used were *Pf* (rFAL 1 TTAAACTGGTTTGGGAAAAC CAAATATATT, rFAL 2 ACACAATGAACTCAATCATGACTACCCGTC), *Pv* (rVIV 1 CGCTTCTAG CTTAATCCACATAACTGATAC, rVIV 2 ACTT CCAAGCCGAAGCAAA-GAAAGTCCTTA), *Pm* (rMAL 1 ATAACATAGTTGTACGTTAAGAATAA CCGC, rMAL 2 AAAATTCCCATGCATAAAAAA TTATACAAA), and *Po* (rOVA 1 ATCTCTTTTGC TATTTTTTAGTATTGGAGA, rOVA 2 GGAAAA GGACACATTAATTGTATCCTAGTG)⁴⁴.

Diagnostic performance, quantitative agreement, and sample size analyses

Microscopy, RDT, and molecular assays were conducted by the Yale and Cameroon teams, who were blinded to the Cytophone results. All samples were classified qualitatively (positive or negative for malaria) and quantitatively (peaks/minute for Cytophone and parasites/mL for microscopy and qPCR). The LoD for the varATS qPCR assay in our study was determined using the mean parasite density and standard deviations of negative control samples and low-concentration samples of cultured 3D7 *Pf* parasites⁴⁵. For speciation, the presence of *Pf*, *Pv*, *Pm*, and *Po* was determined by microscopy and nested PCR. Positive controls for nested PCR included *Pf* strain 3D7 (MRA-102) and 18S

rRNA plasmid DNA for *Pv* (MRA-178), *Pm* (MRA-179), and *Po* (MRA-180) (Bei Resources, Manassas, VA). Highly sensitive varATS qPCR was considered the overall gold standard for *Pf* detection due to its superior sensitivity to current POC diagnostics. Microscopy was considered the gold standard for available POC methods. Rates of concordant and discordant results were used to calculate the sensitivity, specificity, PPV, NPV, and accuracy of each diagnostic. ROC-AUC curves were created to measure the performance in comparison to the gold standard by plotting the true positive rate (sensitivity) against the false positive rate (1-specificity). For each ROC-AUC curve, the AUC was calculated as the diagnostic performance or the probability that the diagnostic will rank a randomly chosen positive sample higher than a randomly chosen negative sample⁵⁸. As a general rule for diagnostic performance, ROC-AUC values of 0.5, 0.51–0.69, 0.7–0.79, and 0.8–0.89 represent a random classifier, poor, acceptable, and excellent performance⁵⁹. Additionally, the Youden index was calculated for all points on the ROC-AUC, with the maximum Youden index value indicating each diagnostics' optimum parasite density cut-off point for identifying varATS-positive samples⁶⁰. The reference diagnostic standard for species detection was nested PCR. The correlation between varATS, microscopy, and Cytophone quantitative results was calculated using linear regression and the Pearson correlation coefficient. A level of agreement analysis was not possible with Cytophone data because the quantitative output is not parasite density. NCSS 2021, v21.0.4 (NCSS, LLC) was used for all diagnostic performance and correlation analyses, and Microsoft® Excel® 2019 MSO (Version 2206 Build 16.0.15330.20260) 64-bit was used to create tables and figures.

For the Hanley-McNeil method of ROC curve area under the curve analysis with continuous data, the sample size to produce a 95% lower confidence bound with a distance of 0.1 from the sample area under the curve of 0.70 (the cutoff for acceptable diagnostic performance) to the lower limit were 116 and 76 for sample malaria prevalence of 25% and 50%, respectively. To accommodate an estimated combined participant dropout, missing visits, and excluded data rate of 20%, we estimated the need to enroll $n = 26$ participants in the longitudinal phase of the study. PASS 2019, v19.0.10 (NCSS, LLC) was used for all sample size and power calculations.

Reporting summary

Further information on research design is available in the Nature Portfolio Reporting Summary linked to this article.

Data availability

The processed data generated in this study are provided in the Source Data file. The raw data are protected and are not available due to data privacy laws. Source data is available at https://figshare.com/articles/dataset/Source_Data_Noninvasive_in_vivo_photoacoustic_detection_of_malaria_with_Cytophone_in_Cameroon/27058834?file=49282834. Source data are provided with this paper.

Code availability

The data were obtained using unique customized software. The (1) Cytophone_Data_Viewer_v6.4.exe, (2) example dataset, (3) installation instructions, and (4) Data Viewer instructions are available at <https://doi.org/10.6084/m9.figshare.26150950>.

References

- World Health Organization. *World Malaria Report 2022* (World Health Organization, Geneva, Switzerland, 2022).
- Phillips, M. A. et al. Malaria. *Nat. Rev. Dis. Prim.* **3**, 17050 (2017).
- Fuehrer, H. P., Campino, S. & Sutherland, C. J. The primate malaria parasites *Plasmodium malariae*, *Plasmodium brasilianum* and *Plasmodium ovale* spp.: genomic insights into distribution, dispersal and host transitions. *Malar. J.* **21**, 138 (2022).
- Murphy, S. C. et al. Malaria diagnostics in clinical trials. *Am. J. Trop. Med. Hyg.* **89**, 824–839 (2013).
- Varo, R., Balanza, N., Mayor, A. & Bassat, Q. Diagnosis of clinical malaria in endemic settings. *Expert Rev. Anti-Infect. Ther.* **19**, 79–92 (2021).
- Roh, M. E. et al. Asymptomatic *Plasmodium* infections in children in low malaria transmission setting, Southwestern Uganda. *Emerg. Infect. Dis.* **22**, 1494–1498 (2016).
- Feleke, S. M. et al. *Plasmodium falciparum* is evolving to escape malaria rapid diagnostic tests in Ethiopia. *Nat. Microbiol.* **6**, 1289–1299 (2021).
- Yerlikaya, S., Campillo, A. & Gonzalez, I. J. A systematic review: performance of rapid diagnostic tests for the detection of *Plasmodium knowlesi*, *Plasmodium malariae*, and *Plasmodium ovale* mono-infections in human blood. *J. Infect. Dis.* **218**, 265–276 (2018).
- Mihreteab, S. et al. Increasing prevalence of artemisinin-resistant HRP2-negative malaria in Eritrea. *N. Engl. J. Med.* **389**, 1191–1202 (2023).
- Bousema, T., Okell, L., Felger, I. & Drakeley, C. Asymptomatic malaria infections: detectability, transmissibility and public health relevance. *Nat. Rev. Microbiol.* **12**, 833–840 (2014).
- Kamaliddin, C. et al. The role of ultrasensitive molecular methods for detecting malaria—the broader perspective. *Clin. Infect. Dis.* **73**, e1387–e1390 (2021).
- Lucchi, N. W. et al. Evaluation of the illumigene malaria LAMP: a robust molecular diagnostic tool for malaria parasites. *Sci. Rep.* **6**, 36808 (2016).
- Hofmann, N. et al. Ultra-sensitive detection of *Plasmodium falciparum* by amplification of multi-copy subtelomeric targets. *PLoS Med.* **12**, e1001788 (2015).
- Adams, M. et al. An ultrasensitive reverse transcription polymerase chain reaction assay to detect asymptomatic low-density *Plasmodium falciparum* and *Plasmodium vivax* infections in small volume blood samples. *Malar. J.* **14**, 520 (2015).
- Murphy, S. C. et al. Real-time quantitative reverse transcription PCR for monitoring of blood-stage *Plasmodium falciparum* infections in malaria human challenge trials. *Am. J. Trop. Med. Hyg.* **86**, 383–394 (2012).
- Sullivan, D. Hemozoin: a biocrystal synthesized during the degradation of hemoglobin. *Biopolymers Online* 129–137 (2005).
- Coronado, L. M., Nadovich, C. T. & Spadafora, C. Malarial hemozoin: from target to tool. *Biochim. Biophys. Acta* **1840**, 2032–2041 (2014).
- Mohapatra, S. et al. Hemozoin pigment: an important tool for low parasitemic malarial diagnosis. *Korean J. Parasitol.* **54**, 393–397 (2016).
- Delahunt, C., Horning, M. P., Wilson, B. K., Proctor, J. L. & Hegg, M. C. Limitations of haemozoin-based diagnosis of *Plasmodium falciparum* using dark-field microscopy. *Malar. J.* **13**, 147 (2014).
- Burnett, J. L., Carns, J. L. & Richards-Kortum, R. Towards a needle-free diagnosis of malaria: in vivo identification and classification of red and white blood cells containing haemozoin. *Malar. J.* **16**, 447–447 (2017).
- Schloetel, J.-G., Heine, J., Cowman, A. F. & Pasternak, M. Guided STED nanoscopy enables super-resolution imaging of blood stage malaria parasites. *Sci. Rep.* **9**, 4674 (2019).
- Frita, R. et al. Simple flow cytometric detection of haemozoin containing leukocytes and erythrocytes for research on diagnosis, immunology and drug sensitivity testing. *Malar. J.* **10**, 74 (2011).
- Rifaie-Graham, O. et al. Hemozoin-catalyzed precipitation polymerization as an assay for malaria diagnosis. *Nat. Commun.* **10**, 1369 (2019).
- Catarino, S. O. et al. Portable device for optical quantification of hemozoin in diluted blood samples. *IEEE Trans. Biomed. Eng.* **67**, 365–371 (2020).

25. Kong, T. F. et al. Enhancing malaria diagnosis through microfluidic cell enrichment and magnetic resonance relaxometry detection. *Sci. Rep.* **5**, 11425 (2015).
26. Chen, K., Yuen, C., Aniweh, Y., Preiser, P. & Liu, Q. Towards ultra-sensitive malaria diagnosis using surface enhanced Raman spectroscopy. *Sci. Rep.* **6**, 20177 (2016).
27. Rebelo, M., Grenho, R., Orban, A. & Hanscheid, T. Transdermal diagnosis of malaria using vapor nanobubbles. *Emerg. Infect. Dis.* **22**, 343–344 (2016).
28. Kumar, R. et al. First successful field evaluation of new, one-minute haemozoin-based malaria diagnostic device. *EClinicalMedicine* **22**, 100347 (2020).
29. Valdivia, H. O. et al. Field validation of a magneto-optical detection device (Gazelle) for portable point-of-care *Plasmodium vivax* diagnosis. *PLoS ONE* **16**, e0253232 (2021).
30. de Melo, G. C. et al. Performance of a sensitive haemozoin-based malaria diagnostic test validated for vivax malaria diagnosis in Brazilian Amazon. *Malar. J.* **20**, 146 (2021).
31. Shapiro, H. M. Flow cytometry: the glass is half full. *Methods Mol. Biol.* **1678**, 1–10 (2018).
32. Shapiro, H. M. *Practical Flow Cytometry* (Wiley-Liss, New York, 1994).
33. Veldhoen, M. E.-I.-C. Guidelines for the use of flow cytometry. *Immun. Inflamm. Dis.* **5**, 384–385 (2017).
34. Tuchin, V. V., Tárnok, A. & Zharov, V. P. In vivo flow cytometry: a horizon of opportunities. *Cytometry A* **79**, 737–745 (2011).
35. Galanzha, E. I. & Zharov, V. P. Circulating tumor cell detection and capture by photoacoustic flow cytometry in vivo and ex vivo. *Cancers (Basel)* **5**, 1691–1738 (2013).
36. Garcia, G. A. et al. Malaria absorption peaks acquired through the skin of patients with infrared light can detect patients with varying parasitemia. *PNAS Nexus* **1**, pgac272 (2022).
37. Cai, C. et al. In vivo photoacoustic flow cytometry for early malaria diagnosis. *Cytometry A* **89**, 531–542 (2016).
38. Galanzha, E. I. et al. In vivo liquid biopsy using Cytophone platform for photoacoustic detection of circulating tumor cells in patients with melanoma. *Sci. Transl. Med.* **11**, eaat5857 (2019).
39. Menyae, Y. A. et al. Preclinical photoacoustic models: application for ultrasensitive single cell malaria diagnosis in large vein and artery. *Biomed. Opt. Express* **7**, 3643–3658 (2016).
40. Nedosekin, D. A., Sarimollaoglu, M., Ye, J. H., Galanzha, E. I. & Zharov, V. P. In vivo ultra-fast photoacoustic flow cytometry of circulating human melanoma cells using near-infrared high-pulse rate lasers. *Cytometry A* **79**, 825–833 (2011).
41. Jawad, H. J. et al. Towards rainbow portable Cytophone with laser diodes for global disease diagnostics. *Sci. Rep.* **12**, 8671 (2022).
42. Zharov, V. P. et al. Infrared imaging of subcutaneous veins. *Lasers Surg. Med.* **34**, 56–61 (2004).
43. Jawad, H. J., Sarimollaoglu, M., Biris, A. S. & Zharov, V. P. Dynamic blood flow phantom with negative and positive photoacoustic contrasts. *Biomed. Opt. Express* **9**, 4702–4713 (2018).
44. Snounou, G. et al. High sensitivity of detection of human malaria parasites by the use of nested polymerase chain reaction. *Mol. Biochem. Parasitol.* **61**, 315–320 (1993).
45. Armbruster, D. A. & Pry, T. Limit of blank, limit of detection and limit of quantitation. *Clin. Biochem. Rev.* **29** (Suppl. 1), S49–S52 (2008).
46. Plowe, C. V., Djimde, A., Bouare, M., Doumbo, O. & Wellems, T. E. Pyrimethamine and proguanil resistance-conferring mutations in *Plasmodium falciparum* dihydrofolate reductase: polymerase chain reaction methods for surveillance in Africa. *Am. J. Trop. Med. Hyg.* **52**, 565–568 (1995).
47. Galanzha, E. I. et al. In vivo magnetic enrichment and multiplex photoacoustic detection of circulating tumour cells. *Nat. Nanotechnol.* **4**, 855–860 (2009).
48. Grobusch, M. P., Hanscheid, T., Zoller, T., Jelinek, T. & Burchard, G. D. Rapid immunochromatographic malarial antigen detection unreliable for detecting *Plasmodium malariae* and *Plasmodium ovale*. *Eur. J. Clin. Microbiol. Infect. Dis.* **21**, 818–820 (2002).
49. Poti, K. E., Sullivan, D. J., Dondorp, A. M. & Woodrow, C. J. HRP2: transforming malaria diagnosis, but with caveats. *Trends Parasitol.* **36**, 112–126 (2020).
50. Mitchell, C. L. et al. Household prevalence of *Plasmodium falciparum*, *Plasmodium vivax*, and *Plasmodium ovale* in the Democratic Republic of the Congo, 2013–2014. *Clin. Infect. Dis.* **73**, e3966–e3969 (2021).
51. Srinamon, K. et al. The prognostic and diagnostic value of intra-leukocytic malaria pigment in patients with severe falciparum malaria. *Nat. Commun.* **13**, 6882 (2022).
52. Bohndiek, S. E., Bodapati, S., Van De Sompel, D., Kothapalli, S. R. & Gambhir, S. S. Development and application of stable phantoms for the evaluation of photoacoustic imaging instruments. *PLoS ONE* **8**, e75533 (2013).
53. Noland, G. S., Briones, N. & Sullivan, D. J. Jr The shape and size of hemozoin crystals distinguishes diverse *Plasmodium* species. *Mol. Biochem. Parasitol.* **130**, 91–99 (2003).
54. Cai, C. et al. Photoacoustic Flow Cytometry For Single Sick Cell Detection In Vitro And In Vivo. *Anal. Cell Pathol. (Amst.)* **2016**, 2642361 (2016).
55. Antonio-Nkondjio, C. et al. Review of malaria situation in Cameroon: technical viewpoint on challenges and prospects for disease elimination. *Parasit. Vectors* **12**, 501 (2019).
56. World Health Organization. *WHO Guidelines for Malaria* (ed. Global Malaria Programme, G.R.C.) (Geneva, Switzerland, 2022).
57. Radfar, A. et al. Synchronous culture of *Plasmodium falciparum* at high parasitemia levels. *Nat. Protoc.* **4**, 1899–1915 (2009).
58. DeLong, E. R., DeLong, D. M. & Clarke-Pearson, D. L. Comparing the areas under two or more correlated receiver operating characteristic curves: a nonparametric approach. *Biometrics* **44**, 837–845 (1988).
59. Hosmer, D. W. & Lemeshow, S. *Applied Logistic Regression* Ch. 5 (John Wiley and Sons, 2000).
60. Youden, W. J. Index for rating diagnostic tests. *Cancer* **3**, 32–35 (1950).

Acknowledgements

We would like to thank the participants in Cameroon, the staff at the University Teaching Hospital of Yaoundé (CHU) and clinics for participant referral, and CHU for the use of their microbiology laboratory. UAMS staff was supported by the UAMS Endowment funds. Funding to J.N.A. and the Cameroonian team was provided by the Downs International Health Student Travel Fellowship, the NIH Fogarty International Center (Grant # D43TW010540, Awardee: J.N.A.), the National Institute of Biomedical Imaging and Bioengineering, and the NIH National Center for Advancing Translational Science (CTSA Grant # UL1 TR001863, Awardee: J.N.A.). Additional support was provided by the National Institute of Allergy and Infectious Diseases (Grant # R21AI160171, Awardee: S.P.).

Author contributions

Y.B., V.P.Z., and S.P. made equal contributions to this work as senior authors. V.P.Z. and S.P. designed the study and wrote the manuscript. Y.B. and L.E. oversaw the study in Cameroon. V.P.Z. and E.I.G. developed the general design and the Cytophone schematics. Q.Z., Y.Z., and R.C. developed a new compact ultrasound transducer design and provided their technical characterization. A.C.Y., Y.A.M., and M.S. developed the Cytophone prototypes and tested technical parameters under V.P.Z. guidance. J.N.A. and S.P. wrote the study protocol. J.N.A. participated in study design, set-up and participant recruitment, conducted molecular assays, performed diagnostic performance analyses, and assisted

in manuscript preparation. K.R., Y.B., L.E., R.N., and S.P. managed regulatory aspects. M.W., A.C.Y., and M.S. handled device shipment. J.-M.N. and Y.T. led on-site conventional malaria diagnostics and phlebotomy. H.K.G. provided access and oversight at the University Teaching Hospital of Yaoundé for patient recruitment. M.S. developed software, performed signal processing, analyzed the Cytophone data, and generated figures. S.U. and M.S. analyzed the signal waveforms and traces. K.M.C. and J.N.A. tested participants with the Cytophone and collected data. A.M. and E.M. conducted clinical assessments and safety follow-ups. A.B. and J.Y.S. formulated and managed technical tasks with a focus on logistics between UALR and UAMS teams.

Competing interests

V.P.Z., J.Y.S., M.S., Y.A.M., E.I.G., and UAMS have a financial interest in the technology discussed in this publication. V.P.Z. and J.Y.S. both have financial interests in CytoAstra, LLC, which has licensed the technology presented in this research work. These financial interests have been reviewed and approved in accordance with the UAMS competing interest policies. The other authors do not have competing interests to disclose.

Inclusion and Ethics

This research is part of a nearly 7-year collaboration between colleagues in Cameroon, the University of Arkansas Medical Sciences, and Yale School of Public Health that has focused on developing a noninvasive diagnostic for malaria. The research is relevant locally and for the detection of malaria throughout sub-Saharan Africa and the malaria-endemic world. Our collaboration is founded on principles of global health equity, with local and international researchers participating and exchanging scientific knowledge bidirectionally throughout the research process, including study design, implementation, data ownership, authorship, and presentation at scientific meetings. Roles and responsibilities of all collaborators were discussed prior to the outset of the research. Ethical approval was obtained from the Yale Human Investigations Committee, National D'Éthique De La Recherche Pour La Santé Humaine in Cameroon and The Centre Hospitalier et Universitaire de Yaoundé.

Additional information

Supplementary information The online version contains supplementary material available at <https://doi.org/10.1038/s41467-024-53243-z>.

Correspondence and requests for materials should be addressed to Vladimir P. Zharov or Sunil Parikh.

Peer review information *Nature Communications* thanks Maggy Sikulu-Lord and the other, anonymous, reviewer(s) for their contribution to the peer review of this work. A peer review file is available.

Reprints and permissions information is available at <http://www.nature.com/reprints>

Publisher's note Springer Nature remains neutral with regard to jurisdictional claims in published maps and institutional affiliations.

Open Access This article is licensed under a Creative Commons Attribution-NonCommercial-NoDerivatives 4.0 International License, which permits any non-commercial use, sharing, distribution and reproduction in any medium or format, as long as you give appropriate credit to the original author(s) and the source, provide a link to the Creative Commons licence, and indicate if you modified the licensed material. You do not have permission under this licence to share adapted material derived from this article or parts of it. The images or other third party material in this article are included in the article's Creative Commons licence, unless indicated otherwise in a credit line to the material. If material is not included in the article's Creative Commons licence and your intended use is not permitted by statutory regulation or exceeds the permitted use, you will need to obtain permission directly from the copyright holder. To view a copy of this licence, visit <http://creativecommons.org/licenses/by-nc-nd/4.0/>.

© The Author(s) 2024